

Laser-driven nonadiabatic electron dynamics in molecules

M. R. MILLER, Y. XIA, A. BECKER,* AND A. JARÓN-BECKER

JILA and Department of Physics, University of Colorado, Boulder, Colorado 80309-0440, USA

*Corresponding author: andreas.becker@colorado.edu

Received 23 November 2015; revised 24 January 2016; accepted 26 January 2016 (Doc. ID 254380); published 7 March 2016

In this review, we briefly summarize more than a decade of experimental and theoretical investigations regarding the nonadiabatic electron response to intense femtosecond duration laser fields in a variety of molecular systems. Historically, experimental signatures of nonadiabaticity have emerged readily in large, conjugated, or multi-electron systems, disrupting fragmentation behavior and modulating observed rates of ionization. As model theoretical studies performed in H_2^+ and other diatomic species show, departure from traditional quasi-static or cycle-averaged descriptions of laser-induced ionization is often necessary to accommodate the rich and frequently counterintuitive electron dynamics that characterize the nonadiabatic response. Nonadiabatic effects such as transient electron localization or the observation of multiple ionization bursts per driving field cycle possess the capacity to modulate the signal of many strong-field physical effects, such as high-order harmonic generation, photoelectron momentum distributions, and molecular fragmentation products. As the advancement of experimental technologies expands the pursuit of laser-driven physics further into the mid-infrared wavelength regime, we suggest that these nonadiabatic effects will become increasingly pronounced and relevant to the imaging and control of a wide array of molecular species. © 2016 Optical Society of America

OCIS codes: (020.2649) Strong field laser physics; (020.4180) Multiphoton processes; (190.4180) Multiphoton processes; (190.7110) Ultrafast nonlinear optics.

<http://dx.doi.org/10.1364/OPTICA.3.000259>

1. INTRODUCTION

Since the advent of the laser in the 1960s, basic research regarding the response of quantum systems such as atoms, molecules, and solids to intense laser fields has led to the discovery of many new aspects of light–matter interaction. At intensities of 10^{12} W/cm², the strength of the interaction between electrons and the incident light field begins to rival that of the Coulomb interaction, so that it can no longer be adequately described as small perturbation to the physics of the quantum system [1]. Novel phenomena such as above-threshold ionization (ATI) [2], high-order harmonic generation (HHG) [3,4], or laser-induced correlated electron emission [5,6] have been predicted, observed, and interpreted as nonperturbative strong-field effects.

The interaction of laser light with atomic systems, and in particular with rare gas atoms, has been studied extensively and is considered to be well understood. Several *ab initio* theoretical techniques as well as systematic approximation methods have been developed and compare well with experimental observations. For example, strong-field ionization of rare gas atoms can be successfully modeled by using the strong-field approximation (SFA, or Keldysh–Faisal–Reiss theory [7–9]) or by quasi-static tunneling models [7,10,11]. These models of atom–field interaction are based on two assumptions: (1) just one of the bound electrons in the

atoms responds to the external field and becomes dynamically active and (2) this electron follows the oscillation of the electric field adiabatically. Consequently, much of strong-field atomic physics relies on a quasi-static interpretation of the interaction of the strong electric field with the atomic potential, assuming, for example, that ionization depends straightforwardly upon a potential barrier strength modulated by a well-characterized electric field.

The response of molecules to a strong electric field exhibits many phenomena that are not encountered in atomic systems due to extra degrees of freedom (rotation and vibration), the multi-center nuclear frame, and a more complicated electronic energy level structure. In particular, strong-field ionization and fragmentation from molecular targets can become significantly more complex than expectations informed by quasi-static or cycle-averaged formulations of electron dynamics would anticipate. For example, electron wavepackets emitted from the different centers in the molecule can interfere destructively leading to a suppression of molecular ionization [12,13]. Besides such structural effects, the proximity of energetic states and the large dipole moments induced by the greater spatial extent of the system and, in some cases, abetted by delocalization of the electron density can result in an enhancement of multi-electron effects as well as induce nonadiabatic electron motion in response to the external field [14–16].

In this brief review we shall focus on one of these new aspects in the interaction of molecules with an intense laser field, namely the transition from an adiabatic to a nonadiabatic response of the electrons to the external field. This nonadiabatic motion frequently either consists of electron flux in opposition of the induced gradient of the electric field accompanied by enhanced ionization, or represents induced localization of the electron density. Such laser-induced nonadiabatic dynamics is capable of modifying the excitation and ionization behavior of the molecular system. Consequently, nonadiabatic electronic effects must be taken into account when attempting to image or control molecular dynamics through ionization or fragmentation. At the same time, characterizing and understanding the nonadiabatic electronic response provides potential avenues to control electron motion or to exploit a subcycle response time to resolve dynamics on their natural attosecond time scale.

We will begin with an overview of observed signatures of non-adiabatic electron dynamics in the ionization and fragmentation patterns of large and highly conjugated molecules as well as related theoretical models. Next, we shall discuss recent theoretical results regarding the analysis of the mechanisms for nonadiabaticity in the simplest molecular system, the hydrogen molecular ion. Finally, we shall focus on the impact of the laser-induced nonadiabatic electron dynamics on a variety of observables. We will end with a brief summary and outlook.

2. INDUCING NONADIABATICITY IN ELECTRON RESPONSE TO STRONG LASER FIELDS

The assumption of an adiabatic electron response in atoms, and specifically in rare gas atoms, is justified in view of the large spacing between electronic energy levels. In contrast, the energy levels of molecules are, in general, energetically much closer. This results in slower electron dynamics than would be expected from atomic systems. Furthermore, it has been argued that as the molecular size increases, the time it takes for an electron to traverse the molecule rivals the period of the laser field, in favor of inducing a nonadiabatic response [16–18].

A. Manifestation of Nonadiabaticity in Large and Highly Conjugated Molecules

The transition from adiabatic to nonadiabatic electron dynamics in large molecules is particularly evinced by highly conjugated systems, as examined by Lezius *et al.* [16,17] for cases of linear conjugated systems, and Markevitch *et al.* [19,20] for aromatic molecules. In Fig. 1 the mass spectra of three linearly, fully conjugated all trans hydrocarbons of increasing length following the interaction with laser pulses at different wavelengths are shown [16].

Two peaks occur in the mass spectrum of the smallest molecule (hexatriene), indicating the stable production of the first two charge states of the parent ion accompanied with little fragmentation. These results are in agreement with the qualitative predictions of the quasi-static ionization picture and, hence, the assumption of an adiabatic electron response to the oscillating electric field of the laser, independent of its period. In contrast, the largest molecule (β -carotene) shows a mass spectrum indicative of persistent nonadiabatic electron dynamics through extensive fragmentation of the molecule at both wavelengths considered. Most interesting in the present context is the strong

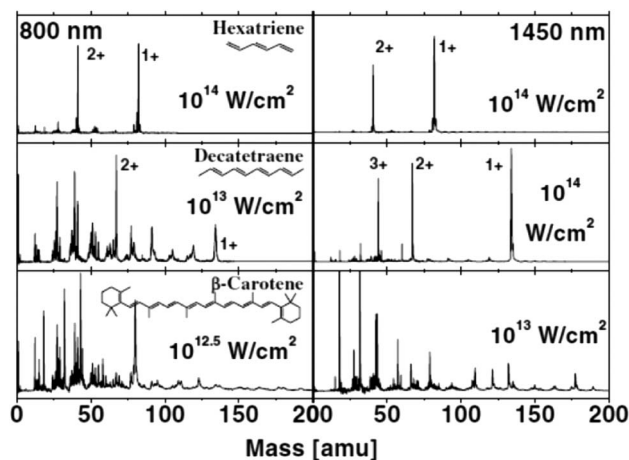


Fig. 1. Ionization and fragmentation patterns represented by the mass spectra of hexatriene, decatetraene, and β -carotene for the interaction with laser pulses at 800 and 1450 nm. Figure reprinted with permission from Lezius *et al.*, *Phys. Rev. Lett.*, **86**, 51 (2001) [16]. Copyright 2001 by the American Physical Society. <http://journals.aps.org/prl/abstract/10.1103/PhysRevLett.86.51>

wavelength-dependent variation of the mass spectrum of decatetraene, which exhibits population of the singly, doubly, and triply charged parent ion at 1450 nm, but demonstrates strong fragmentation at the shorter wavelength of 800 nm. It was pointed out by Lezius *et al.* that this observation suggests a transition from the adiabatic single-active electron picture to a nonadiabatic multi-electron ionization dynamic. At 800 nm, the duration of the field oscillation was argued insufficient for the electron to traverse the large molecule adiabatically. In contrast, the longer field cycle of 1450 nm did afford the electron wavepacket sufficient response time, resulting in the stable production of a few charge states. Similar strong variations in the ionization and fragmentation patterns have been observed for aromatic molecules at a given wavelength for rather small variations of the laser intensity [19,20].

B. Intramolecular Nonadiabatic Behavior in Small Conjugated Molecules

Following qualitative considerations about the role of Landau–Zener-type transitions [16,17], a model was introduced to describe the onset of the transition from adiabatic single-active electron to nonadiabatic multi-electron dynamics through a coupling of the ground state and the low-lying excited states in molecules [19,20]. According to this model, the strongest of these transitions involves a charge-transfer state as a doorway state. Further elements of the theory take into account the multi-electron nature of the polyatomic molecules used in related experiments.

Advanced theoretical studies regarding the nonadiabaticity of the electronic response in polyatomic molecules to strong laser fields have been performed using methods of time-dependent configuration interaction with single excitations (TD-CIS) and time-dependent Hartree–Fock theory [21–26]. In these studies, simulations are typically performed under so-called nonionizing conditions, in which the continuum is not taken into account. Signatures of adiabatic versus nonadiabatic dynamics can be observed via properties of the molecule, such as the instantaneous

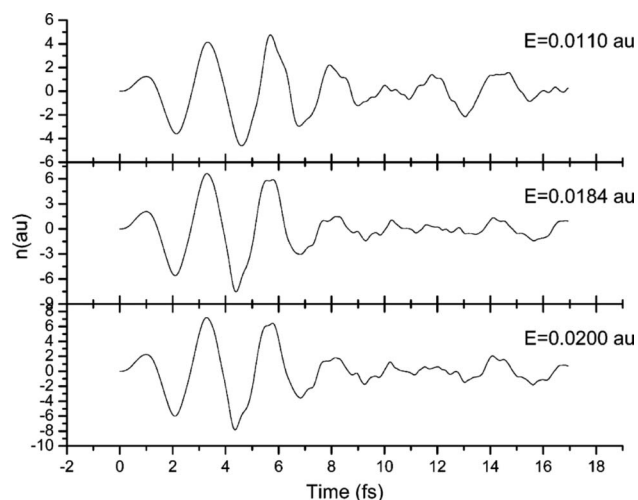


Fig. 2. Results of time-dependent Hartree–Fock simulations for the interaction of the anthracene $1+$ cation with strong electric fields of different intensities. The instantaneous dipole response in each case shows a nonadiabatic behavior, and the frequency composition of the residual dipole moment is determined by the field strength used. The total pulsewidth of the laser field is ~ 7 fs. Reprinted with permission from Smith *et al.*, J. Phys. Chem. A, **111**, 6920 (2007) [24]. Copyright 2007 by the American Physical Society.

dipole, the charge distribution on each atom (using the Löwdin population analysis), and the orbital occupations. The responses of different groups of molecules have been studied, such as di- and triatomic [21,25], linear polyenes [22,25] and their cations [23], as well as polyacenes [24].

In Fig. 2 an example of the results for the case of the anthracene $1+$ cation driven by laser fields of different intensities is presented. The nonadiabatic response to the electric field is apparent in the instantaneous dipole response via the subcycle oscillatory dynamics. Moreover, dipole response oscillations continue after the end of the pulse and are reminiscent of the (nonadiabatic) excitation in the linear polyene. In qualitative agreement with previous experimental results [16,17,19,20], it is found that the nonadiabatic effects increase with the length (size) of the molecule, they are stronger in the cation than in the neutral molecules, and they get stronger with the increase of the laser intensity.

C. Double Series in ATI Spectra and Fractional Harmonics

Nonadiabatic electron dynamics in molecules can be related to a strong coupling between two states in the molecule. In the case of multi-electron atoms, nonadiabatic laser-driven coupling has been studied in a two-electron two-center reduced dimensionality model [27] and by employing time-dependent density functional theory [28]. Novel features in photoelectron emission spectra (ATI spectra) and HHG spectra in the presence of strong coupling have been reported recently.

In [27] two combs of peaks are observed for the ATI spectra, resulting from calculations using a two-electron two-center model in reduced dimensions. The two series are explained by the coupled population of the two lowest ionic states in the model. As the dynamics change from adiabatic to nonadiabatic behavior the two combs get mixed and can no longer be separated, since

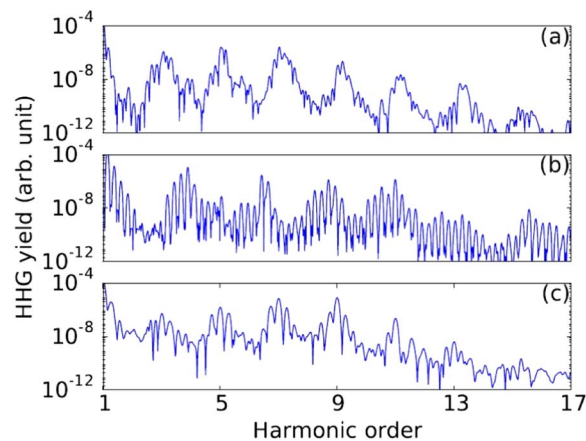


Fig. 3. High harmonic spectra showing fractional harmonics for (a) NO_2 at 400 nm, 10^{14} W cm^{-2} , and 40 fs pulse length; (b) CO_2^+ at 350 nm, 10^{14} W cm^{-2} , and 34 fs; and (c) C_2H_4^+ at 400 nm, 10^{14} W cm^{-2} , and 18 fs [28].

the nonadiabaticity introduces a subcycle time scale. Thus, the ATI electrons carry signatures of the ionization of both states leading to the mixing of the peaks in the two series.

Furthermore, when the driving laser wavelength is tuned to the transition between an inner valence orbital and a hole in the highest occupied molecular orbital, fractional harmonics are found. These harmonics show up as sidebands to the usual integer harmonics and are indicative of the presence of strong coupling and related nonadiabatic dynamics [28]. The underlying mechanism is analogous to that responsible for Mollow sidebands in quantum optics [29]. While first predicted to occur in H_2^+ at extended internuclear distances [30,31], it is now found that this phenomenon is a much more general feature present for other open shell molecules even at equilibrium geometry. Figure 3 shows examples of the fractional harmonics for three open shell molecule and molecular ions [28]. Depending on the coupling strength, the sidebands are predicted to occur as separate fractional harmonics (as seen for CO_2^+) or merely via a broadening of the odd harmonics (as shown for NO_2).

3. MECHANISMS FOR NONADIABATICITY IN THE HYDROGEN MOLECULAR ION

Remarkably, signatures of nonadiabatic dynamics similar to those seen in multi-electron systems arise in single-electron molecules as well. In this section, we explore nonadiabatic enhanced ionization and transient electron localization behaviors in the hydrogen molecular ion (H_2^+) as a simple and representative model. The reduced number of spatial dimensions needed to represent this system makes it highly amenable to theoretical treatment in contrast to larger molecular targets. Numerically, H_2^+ is fully treatable from *ab initio* principles; in addition, the predominant participation of the ground ($|g\rangle$) and first excited state ($|u\rangle$) when driven by strong near- and mid-infrared (IR) laser pulses permits rigorous theoretical treatment. In the following, we examine theoretical developments regarding the rich and frequently counterintuitive behavior of an electron driven by a strong laser field in H_2^+ , revealing fundamental physical mechanisms behind these behaviors and remarking upon theoretical explorations of how these behaviors can be controlled and imaged.

A. Charge-Resonance-Enhanced Ionization

As first identified by Mulliken [32], symmetric molecular ions such as H_2^+ possess pairs of charge-resonant states that, at large internuclear distance (R_0), become nearly degenerate and couple strongly to electromagnetic fields. Further investigations using H_2^+ as a model system have elucidated the important role these states play in the process of laser-induced ionization [14,15], with similar effects observed in experiments involving the higher charge states of CO_2 [33]. In particular, theoretical predictions show that the charge-resonant states can amplify the rate of ionization of H_2^+ by one to three orders of magnitude in models including both electronic and nuclear motion [34]. Throughout an interval of internuclear distances preceding dissociation, the $|g\rangle$ and $|u\rangle$ states of H_2^+ , which possess opposite parity, act as a charge-resonant pair.

The relevancy of this coupling is obvious in the quasi-static picture of ionization at the peak of the electric field. Near its equilibrium internuclear distance, H_2^+ ionizes predominantly from the downhill well through a mechanism analogous to adiabatic single-active electron atomic ionization. However, as the internuclear distance increases, the electric field alters the shape of the barrier between nuclear wells. The shifted energy level of the uphill state enables shorter tunneling times or promotes population immediately into the continuum. This scenario is portrayed in Fig. 4 in the case of a static electric field. When $R_0 = 6.0$ in panel (a), the intramolecular potential barrier is suppressed beneath the energy of the uphill state, resulting in the dramatically increased ionization rate shown in Fig. 4(d) [14]. As R_0 continues

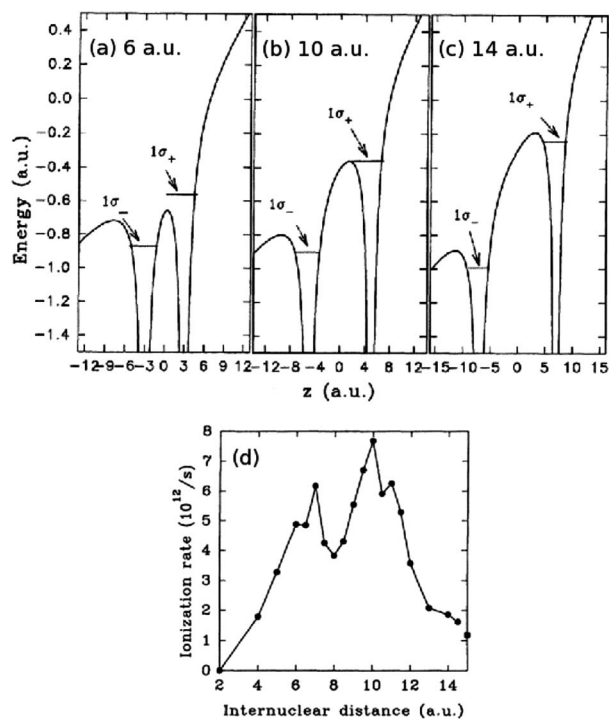


Fig. 4. Charge-resonance-enhanced ionization in H_2^+ is attributable to the energy level structure of the two lowest states of H_2^+ , which are pictured at a peak field strength of $10^{14} \text{ W cm}^{-2}$ when (a) $R_0 = 6.0$, (b) $R_0 = 10.0$, and (c) $R_0 = 14.0$ a.u. along the laser polarization axis z . In (d), theoretical predictions for the ionization rate for a $10^{14} \text{ W cm}^{-2}$, 1064 nm laser source spanning an interval of internuclear distances. Figures adapted with permission from Zuo and Bandrauk, *Phys. Rev. A*, **52**, R2511 (1995) [14]. Copyright 1995 by the American Physical Society.

to increase, the barrier reasserts itself [Fig. 4(b)] until ionization from the uphill well is ultimately again suppressed [Fig. 4(c)]. This situation results in the charge-resonance-enhanced ionization (CREI) effect [14,15] throughout a critical region of internuclear distances shown in Fig. 4(d). The prominent double-peak structure in the ionization rate as a function of internuclear distance has recently been observed experimentally [35]. This field-induced electron nonadiabaticity also imprints signatures upon the HHG spectra of dissociating H_2^+ , where the amplified ionization along the falling part of the driving field results in an overall redshift of harmonic peak locations [36].

The strong enhancement of the ionization signal due to CREI suggests that most strong-field-induced signals will be dominated by dynamics occurring throughout the CREI regime. This is particularly important in the context of resolving nonadiabatic behavior, as in addition to an obvious enhancement of ionization, CREI coincides with a modification of the localization behavior of the electron between the two nuclei. Early predictions of this effect suggested that the near degeneracy of the relevant energy levels enabled population to be preferentially trapped in the uphill well [15]. More recently, it has been proposed that additional ionization channels involving excitation followed by ionization from either site of the molecule may contribute to this quasi-static picture [37]. In addition, numerical results showed evidence that the inversion symmetry of the electron density was broken during laser propagation, potentially enabling the production of even harmonics in HHG spectra [14].

B. Transient Electron Localization

The importance of nonadiabatic electron behavior has become increasingly obvious with time-resolved examination of electron dynamics occurring in the CREI regime, where the quasi-static description of electron behavior has proven incomplete [38]. In fact, time-resolved studies of ionization in H_2^+ and electron behavior therein demonstrated not only that ionization was enhanced but also that the timing of peak ionization could be changed: at laser parameters supporting nonadiabatic behavior, ionization no longer occurred with maximum amplitude near the electric field peak. Instead, several discrete bursts of ionization occurred throughout each half-cycle of the driving laser field (see Fig. 5, [39]).

Analysis of the time-dependent electron density distribution in H_2^+ illustrates that bursts of ionization are accompanied by a transient electron localization upon alternating nuclear centers several times per half-field cycle of the driving laser field [38–41].

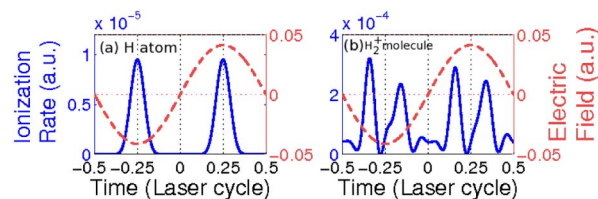


Fig. 5. Theoretical predictions of the ionization rate of (a) hydrogen and (b) H_2^+ with $R_0 = 7.0$ are pictured when driven by 800 nm light with peak intensity $6 \times 10^{13} \text{ W cm}^{-2}$. In hydrogen, ionization is observed to peak when the electric field (red dashed line) is strongest. In contrast, H_2^+ evidences discrete bursts of ionization with strong suppression during the electric field maxima. Figure adapted with permission from Takemoto and Becker, *Phys. Rev. Lett.*, **105**, 203004 (2010) [39]. Copyright 2010 by the American Physical Society.

This dynamic drives population toward the uphill potential well, from which it can be efficiently and rapidly ionized. This dynamic is highly sensitive to the strength and frequency of the electric field used. Different wavelengths or field strengths result in different numbers of localizations during each half-laser cycle, so that selection of the appropriate wavelength enables the localization of the wavefunction counterintuitively and predominantly on the uphill well, reminiscent of the modulated charge distribution described in [22].

Several theoretical justifications for this counterintuitive behavior exist. The likelihood of encountering the electron in the laser polarization direction (z) with a particular momentum (p_z) can be captured through use of the Wigner quasi-probability distribution, which can be calculated as [42]

$$W(z, p_z; t) = \frac{1}{\pi} \iint \rho d\rho dR \int_{-\infty}^{\infty} dy \Psi^*(R, z + y, \rho; t) \times \Psi(R, z - y, \rho; t) \exp(2ip_z y). \quad (1)$$

The results of this analysis for a model 1D H_2^+ system are reproduced in Fig. 6 [40]. The sequence of subpanels shows snapshots of the time evolution of the quasi-probability density, with positive quasi-probabilities encoded in red and negative in blue. In Fig. 6(a), the distribution is plotted at an instant when the electric field crosses zero. The structure of the electron density shows an inherent interference structure due to participating molecular orbitals. This interference pattern is seen to favor transfer of electron density from one side of the molecule (at $z = -3.5$ a.u.) to the other (at $z = 3.5$ a.u.) with $p_z \approx 0.2$ a.u. As

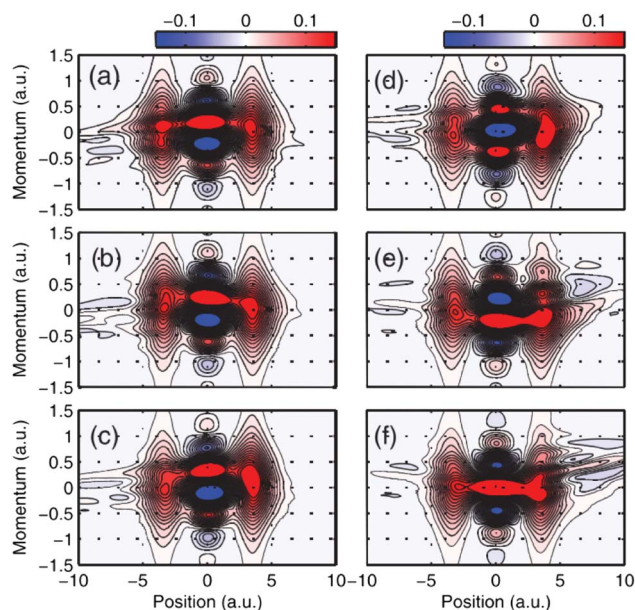


Fig. 6. Wigner distribution of the electron wavefunction of H_2^+ shows the transfer of electron population between nuclear wells, and is depicted for six instances of time spanning a quarter cycle of the driving field, beginning with $E(t) = 0$ in panel (a) and concluding with $E(t) = -E_{\max}$ in panel (f). The respective snapshots are taken at times (in field cycles) (a) $t = -0.500$, (b) $t = -0.450$, (c) $t = -0.400$, (d) $t = -0.351$, (e) $t = -0.301$, and (f) $t = -0.251$. Red sections in the distribution indicate areas where the electron is likely to be found. Figure reprinted with permission from Takemoto and Becker, Phys. Rev. A, **84**, 023401 (2011) [40]. Copyright 2011 by the American Physical Society. <http://journals.aps.org/pr/abstract/10.1103/PhysRevA.84.023401>

transfer at other momenta values is otherwise suppressed, this region of positive electron density is termed a momentum gate (MG) [42], which in subsequent subpanels is shifted by the action of the field vector potential $A(t)$ to values $p_{MG} \rightarrow p_{MG} - A(t)/c$. In the example shown, the driving field is the same as in Fig. 5, and the MG cycles through momentum space in a quarter of the driving field. Consequently, population is driven to the uphill well more rapidly, leading to the quarter-cycle bursts of ionization seen in Fig. 5(b). Additionally, by increasing the wavelength or intensity, the number of localizations would be expected to increase due to the heightened modulation of the position of the MG.

The spatial behavior of the wavefunction can be alternatively understood through the use of Bohmian trajectories. In this representation [41], the behavior of the electron is described by an ensemble of semi-classical trajectories $\{z_j(t) | j = 1, \dots, N_{\text{traj}}\}$ that solve the equations of motion

$$\frac{dz_j}{dt} = v(z_j(t), t) = \frac{\partial S(z_j, t)}{\partial z}. \quad (2)$$

It relates the velocity field $v(z(t), t)$ of each trajectory to the complex phase of the electron wavefunction expressed as

$$\Psi(z, t) = C(z, t) \exp(iS(z, t)), \quad (3)$$

where $C \geq 0$ and $S \in \mathbb{R}$.

A demonstration of the Bohmian trajectory analysis for H_2^+ is shown in Fig. 7 throughout the central cycle of a 10-cycle laser field with peak intensity $4 \times 10^{13} \text{ W cm}^{-2}$ and wavelength 1064 nm. The plotted trajectories represent the motion of the electron wavepacket within the molecule. In Fig. 7(a), both rescattering events and laser-induced intramolecular dynamics are

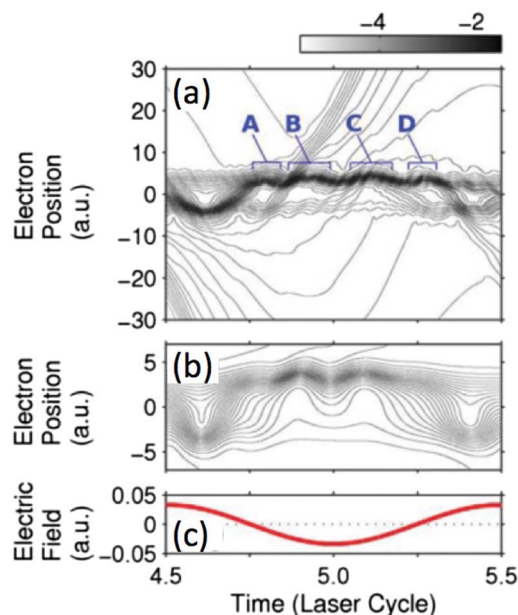


Fig. 7. Bohmian trajectories visualize the behavior of the electron when driven by an intense laser field. In (a), quantum trajectories near protons located at $z = \pm 3.5$ a.u. are plotted over the central field cycle, demonstrating bursts of ionization at time points A–D. Absorbing departing electron trajectories at 7 a.u. isolates intramolecular dynamics from rescattering trajectories, clarifying the transient localization of the electron. The laser field driving this behavior is reproduced in (c). Reprinted with permission from Takemoto and Becker, J. Chem. Phys., **134**, 074309 (2011) [41]. Copyright 2011, AIP Publishing LLC.

implicated in the transport of electron density away from the nuclei of the molecule at time points A–D. Applying an absorbing boundary to the calculation isolates trajectories involved with transient localization and reconstructs laser-driven subcycle localization at time points B and C. Departing wavefunction population at these time points leads to the bursts of ionization exhibited in Fig. 5.

Additionally, in the Bohmian trajectory framework, moments of localization occur when the velocity field across the molecule crosses zero. Similarly, efficient transport of electron density will occur when this velocity field is large. The connection between the phase of the wavefunction and the velocity field provides a means of analyzing the localization behavior further in numerical calculations, where the phase of the wavefunction can be easily obtained. Examining the phase gradient across H_2^+ corresponds well with the behavior of the electron as it traverses the molecule: moments of localization are observed when this gradient is zero. As demonstrated in [41], transient electron localization can be understood as a consequence of the phase of the wavefunction at either nuclear center becoming advanced or retarded in comparison with that of the other center.

The timings of transient electron localization in H_2^+ can be more rigorously developed by modeling the electron response as a nonresonantly driven two-level system. At extended internuclear distances, the $|g\rangle$ and $|u\rangle$ states are energetically well-separated from higher lying excited states; additionally, as the molecule dissociates and passes through the CREI regime, these states become nearly degenerate with energy spacing less than the photon energy of a driving IR source. Under these conditions, as shown in [43], the time evolution of the electron wavefunction can be expanded in a basis of Floquet states to identify moments in time at which the electron maximally occupies the nucleus on the positive or negative side of the grid. These events are seen to occur when the vector potential $A(t) = A_0 \sin \omega t + \phi$ satisfies [39]

$$A(t_{\text{loc}}) = \frac{m\pi + \xi}{2d_{gu}}, \quad \text{with } m = 0, \pm 1, \pm 2, \dots \quad (4)$$

The time instants depend on the mixing angle ξ of the two Floquet states as well as the dipole transition matrix element d_{gu} between the two states. We also remark that in the Floquet treatment the static localization of the electron, as discussed in the original CREI picture [14], occurs in the zeroth-order term of the expansion, while the subcycle transient localization is represented by the next-order term.

Here, we again note the strong dependence of the localization events upon the selection of laser field parameters. Increasing the intensity or the wavelength of the laser used also increases the nonadiabaticity of the resultant behavior, characterized by an increasing number of localizations per half-field cycle. We thus expected that nonadiabatic electron behaviors such as transient localization will be increasingly experimentally relevant as femtosecond laser technology extends more deeply into the mid-infrared regime.

4. DETECTION OF NONADIABATIC INTRAMOLECULAR DYNAMICS

Having established and characterized nonadiabatic electron behavior in H_2^+ , we now focus upon recent theoretical and experimental studies that explore the detection of transient electron

localization in H_2^+ . As we have noted, ionization is the initiator of many strong-field physical effects. We discuss how the strong modulation of ionization exhibited by systems undergoing transient localization renders this signal readily detectable in a variety of strong-field-induced phenomena such as photoionization, molecular dissociation, and HHG. To this end, we review a variety of studies that have focused upon these effects to identify and quantify signatures of transient electron localization in experimental observables. In addition to characterizing the nonadiabatic behavior of the electron, we note that studies performed regarding the physically simple system of H_2^+ are a useful method to distinguish signatures of electron localization from different forms of nonadiabaticity arising from many-body mechanisms. In addition, these studies provide a foundation to observe dynamics occurring on the attosecond scale, positioning such methods at the forefront of attosecond science.

A. Time-Evolving Double-Slit Interference

The laser-driven transient localization of the electron in H_2^+ results in a quickly varying asymmetry of the electron density. Probing of such an asymmetry has been first proposed via the application of a second attosecond pulse with polarization direction along the molecular axis [44,45]. Following adiabatic quasistatic considerations, the generated photoelectron yield along the polarization direction reflects the asymmetry of the electron density, which has been confirmed in theoretical calculations.

This theoretical concept has been later extended by setting the polarization axis at an angle, best perpendicular, to the molecular axis. As first pointed out by Cohen and Fano [46] the resulting emission of partial electron waves from the two atomic centers is conceptually equivalent to the emerging coherent light waves from a double slit in Young's experiment [47]. The asymmetry resulting from the transient localization of the electron density inside H_2^+ can be viewed in analogy to a modulation of the light intensity at the two holes. Consequently, the interference pattern in the photoelectron momentum distribution (PMD) changes with the motion of the electron in the molecule. Numerical calculations [39] have revealed the potential to reconstruct the time-dependent population in the charge-resonance states and, hence, the electron density from the time-evolving momentum distributions.

B. Photoelectron Distribution Following Ionization with Circularly Polarized Light

Ionization of atomic and molecular systems using circularly or elliptically polarized light can be used to extract timing information regarding the ionization event [48]. According to a quasistatic picture of ionization, ionization is expected to peak when the electric field is strongest. When using elliptically polarized light to investigate atomic targets, this affords maximal ionization along the major polarization axis. For diatomic molecular systems, circularly polarized light similarly ionizes most efficiently along the molecular symmetry axis. In each case, the PMD can be collected and analyzed to reconstruct the momentum with which photoelectrons were released, indicative of the electric field present during ionization. Coincidence measurements of the times of flight and positions of both the electron and protons enable the reconstruction of the internuclear distance at the time of ionization as well. In the particular case of H_2^+ , for which the nonadiabatic electron dynamics expected are sensitive to the inter-

nuclear distance of the molecule, this enables an analysis that connects the transient electron localization to modifications of the ionization signal.

This procedure has been theoretically and experimentally studied as a means to image the bursts of ionization that emerge during transient electron localization. As these ionization events no longer coincide directly with the peak of the interacting electric field, the PMD is expected to rotate in momentum space, corresponding to a delay in the timing of peak ionization. This effect was measured in [49], and is shown in Fig. 8. Additional comparisons to simulations using the 2D time-dependent Schrödinger equation (TDSE) and predictions from quasi-static ionization were performed in this study. The dependence of the experimental results and respective theoretical predictions upon internuclear distance is compared in Fig. 8(b). The simple formulation of quasi-static ionization of a molecular target by a circularly polarized field yields a constant angular distribution, in contrast to the internuclear distance-dependent experimental results and numerical calculations. The numerical prediction approximates the response of H_2^+ in the experimental system, suggesting that the inclusion of nonadiabatic electron behavior is critical to accurately reproduce photoionization behavior in H_2^+ .

Further theoretical studies investigated the departure of PMDs from the quasi-static tunnel ionization model and found that the

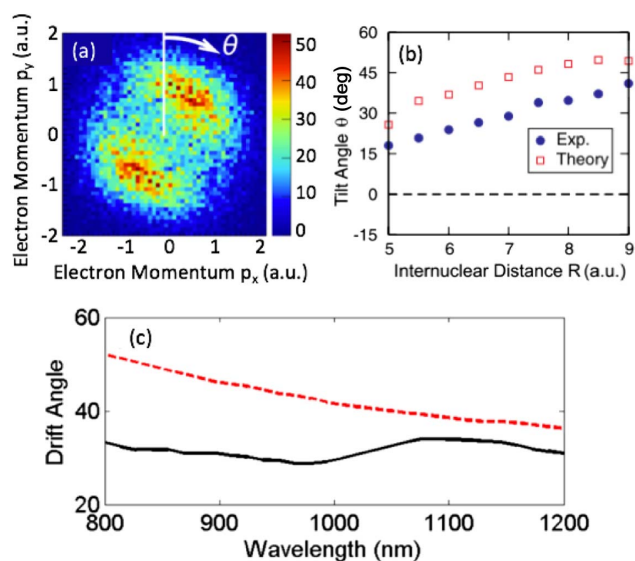


Fig. 8. Rotation of the PMD due to nonadiabatic dynamics that shift the timing of ionization. In (a), the experimental PMD from H_2^+ is shown integrated over the internuclear coordinate and p_z directions. In (b), experimental results (blue circles) and TDSE predictions (red squares) for the angular displacement of the PMD are shown in comparison with the quasi-static ionization prediction (dashed line). The results of further theoretical studies in (c) indicate that the angular displacement of the PMD of H_2^+ (solid black line) is sensitive to the wavelength of the driving field used due to transient electron localization, in contrast to adiabatically responsive atomic hydrogen (red dashed line). Panels (a) and (b) reprinted with permission from Odenweller *et al.*, Phys. Rev. Lett., **107**, 143004 (2011) [49]. Copyright 2011 by the American Physical Society. <http://journals.aps.org/prl/abstract/10.1103/PhysRevLett.107.143004>. Panel (c) reprinted with permission from He *et al.*, Phys. Rev. A, **91**, 063413 (2015) [50]. Copyright 2015 by the American Physical Society. <http://journals.aps.org/pra/abstract/10.1103/PhysRevA.91.063413>

long-range Coulomb interaction plays an essential role in determining the angular distribution of both atomic and molecular PMDs. In [50], numerical calculations were completed using a screened Coulomb potential, with a cut-off implemented at different radial distances. Extending the interaction range of the Coulomb potential introduced a drift angle θ into the final distribution of H_2^+ ionized by circularly polarized light and atomic hydrogen ionized by elliptically polarized light. The behavior of this feature when the wavelength of the ionizing field varied was also investigated for a laser with intensity $6 \times 10^{13} \text{ W cm}^{-2}$, the results for which are reproduced in Fig. 8(c). In these results, hydrogen (red dashed line) serves as a reference of adiabatic behavior: as wavelength is increased, the drift angle monotonically decreases due to an increasing excursion distance from the parent ion. In contrast, the drift angle accumulated in the PMD of H_2^+ is nonmonotonic, which is connected to fluctuations in the timing of peak ionization depending on the wavelength of the laser source used. Transient electron localization determines the moment at which the electron is most localized upon the uphill well of the H_2^+ , from which ionization occurs, influencing the appearance of the resultant PMD.

C. Control Over Fragmentation

The formation and breakage of chemical bonds during chemical reactions is mediated by the correlated motion of electrons and nuclei: controlling electron motion can thus be seen as a means to control chemical reactions. The development of strong-field lasers with subfemtosecond duration made it feasible to image a variety of fundamental processes relevant to the electronic dynamics exhibited by a system undergoing a chemical reaction, such as dissociation. Dissociating molecules undergo complex electronic behavior rendering a full understanding of the process difficult to obtain. Consequently, theoretical studies regarding H_2^+ serve as an important prototype for the complex dynamics expected by incorporating additional bodies or degrees of freedom into the system.

Even in the relatively simple case of H_2^+ , however, the final dissociation probability is complicated considerably by ongoing transient localization of the electron wavefunction in response to driving the dissociation by a strong laser field. In Fig. 9, the modification of the final electron distribution can be seen to be influenced strongly by laser intensity, and correspondingly by the induced nonadiabatic electron dynamics. Based on numerical calculations involving 2D electron motion and an additional nuclear degree of freedom [42], driving H_2^+ with the same laser profile (wavelength, envelope, and number of cycles) while changing the intensity of the field afforded control over the relative population of the two dissociating nuclei. In this study, an initial UV field was introduced to populate the dissociating $2p\sigma_u$ state from the molecular ion prepared in the nondissociating $1s\sigma_g$ state; the total dissociating wavepacket was extracted through projection onto $2p\sigma_u$, and subsequently integrated over positive and negative space in the laser polarization direction to evaluate the relative probabilities of occupying either nucleus during and following interaction with an 800 nm laser field.

For the pulse profile depicted in Fig. 9(a), the results of driving with three different intensities are shown in Figs. 9(b)–9(d). Transitioning from a field intensity of $3 \times 10^{12} \text{ W cm}^{-2}$ [Fig. 9(b)] to the moderately more intense case of $2 \times 10^{13} \text{ W cm}^{-2}$ [Fig. 9(c)] reverses the ultimate direction favored by the electron, while a

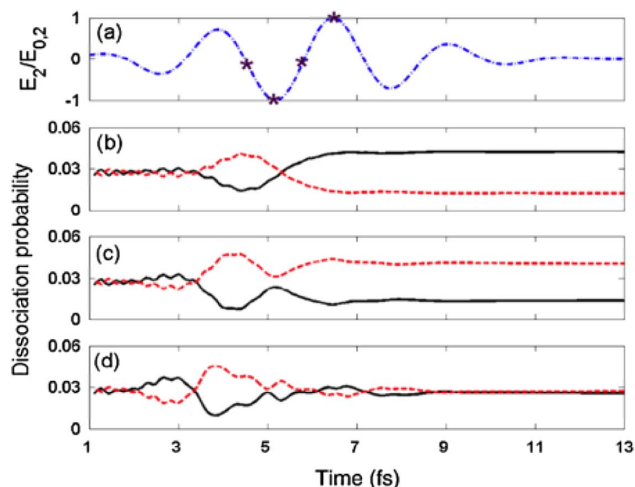


Fig. 9. Subsequent to UV-laser-induced population of the dissociating $2p\sigma_u$ state, H_2^+ is driven with an IR laser source with a profile as shown in (a). The electron density occupying the positive (red dashed line) and negative (black solid line) spatial regions is shown during and following interaction with a laser field of intensity (b) $3 \times 10^{12} \text{ W cm}^{-2}$, (c) $2 \times 10^{13} \text{ W cm}^{-2}$, and (d) $10^{14} \text{ W cm}^{-2}$. Comparison of results following field interaction (e.g., at 10 fs) shows that the dissociation product distribution is highly influenced by the laser intensity selected due to the participation of transient electron localization. Figure reprinted with permission from He *et al.*, Phys. Rev. Lett., **101**, 213002 (2008) [42]. Copyright 2008 by the American Physical Society. <http://journals.aps.org/prl/abstract/10.1103/PhysRevLett.101.213002>

further increase to $10^{14} \text{ W cm}^{-2}$ favors each nucleus evenly. This surprising dynamics is a direct result of the nonadiabatic intramolecular electronic response induced by the electric field. As H_2^+ fragments, the electron is initially free to traverse between nuclei. However, the potential barrier between the centers increases with nuclear separation, ultimately confining the electron to occupy one of the two centers. In a system for which the electron followed the laser field adiabatically, the final distribution of the electron would be expected to consistently reflect the laser profile selected; in the present case, within which transient localization plays an important role, the electron may be driven to favorably occupy one side of the molecule. As this particular case shows, inducing nonadiabatic transient localization thus allows laser intensity to be potentially used as a tunable means for producing a desired dissociation product.

D. Spectral Minima in High-Order Harmonic Generation

The capacity of laser-driven electron localization to modify the timing of ionization also has profound implications for experimentally observable signals that rely upon strong-field ionization. HHG is an excellent example of such a process. Conventionally, HHG is described through a three-step mechanism [51,52], through which an electron is first tunnel-ionized, is next accelerated from the parent ion, and then finally returns, recombining with the parent ion and releasing energy gained during acceleration through a high-energy photon. In total, this process typically yields an energy spectrum extending through odd harmonics of the driving field with constant efficiency up to a well-defined cut-off frequency.

The amplitude of yield into each harmonic may also be considered representative of electron dynamics during each step of

the process. Consequently, HHG is commonly used to image molecular systems by identifying energetic regions of suppressed harmonic emission and connecting these minima to features of the molecular target. Nuclear dynamics and the structure of diatomic targets, for example, have been theoretically [53–55] and experimentally [56–65] measured by observing a two-center interference mechanism occurring at the time of recombination, relating the deBroglie wavelength of the returning electron to the distance separating the nuclear centers at the time of ionization. Minima have also been identified due to an accumulated phase difference in the propagated and residual electron wavepackets, constituting a form of imaging changes in the molecular excited state orbitals during the electron's excursion from the parent ion [66–70].

Each of these mechanisms depends, entirely or in part, upon the electron's recombination with the parent ion. In contrast, the laser-driven transient localization of the electron in H_2^+ highly influences the ionization behavior of the electron, and is correspondingly fundamentally interesting in the context of HHG as a test of the role that ionization plays on the structure of the total HHG signal. Additionally, the temporal resolution afforded by the HHG signal—different moments of ionization contributed to the amplitude of different harmonics—constitutes a means of directly imaging the ionization, and hence intramolecular dynamics, of the electron within H_2^+ at extended internuclear distances, as recently proposed [71].

An example of the total HHG signal generated by simulating H_2^+ in 3D with fixed nuclei arranged at $R_0 = 7$ is shown in Fig. 10(a) [71]. The molecular ion is driven by a laser with intensity $6 \times 10^{13} \text{ W cm}^{-2}$, and with wavelength $\lambda = 1400 \text{ nm}$.

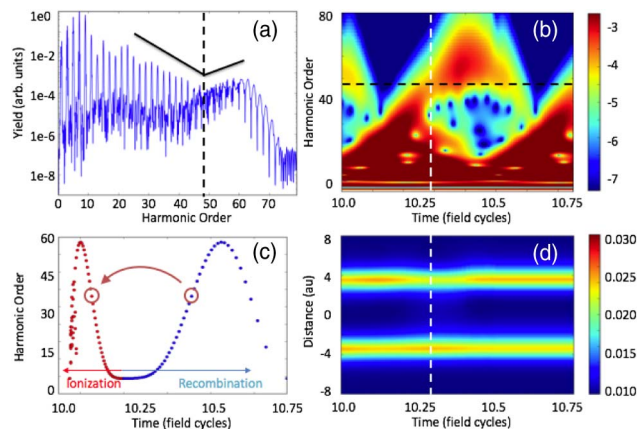


Fig. 10. Theoretical calculations of the HHG spectrum emitted by fixed nuclei H_2^+ at $R_0 = 7.0$ driven by a 1400 nm, 20-cycle full width source with intensity $6 \times 10^{13} \text{ W cm}^{-2}$ are shown in (a). The position of the minimum is marked by the dashed line; the overall modulation of the high-energy plateau is demonstrated by lines superimposed above the spectrum. In (b), the temporal origin of the minimum is investigated through a time-frequency analysis (TFA) of emission during recombination throughout a center cycle of the driving field. A minimum is found in the TFA at the same energetic location as the full HHG spectrum. (c) A classical analysis maps emission at recombination to approximate the moment of ionization of the electron wavepacket, enabling reconstruction of the electron density (d) during ionization corresponding to times of recombination in the TFA. The minimum feature is seen to coincide with maximal localization upon the downhill well. Panels (a) and (b) adapted with permission from Miller *et al.*, Phys. Rev. A, **93**, 013406 (2016) [71]. Copyright 2016 by the American Physical Society.

The lineshape of the strongly modulated structure of the high-energy plateau is indicated by the black lines superposed above the spectrum. In contrast to the flat plateau resulting from a prototypical atomic subject, this spectrum features a pronounced minimum. The energetic position of the minimum does not agree with predictions corresponding to known structural or dynamical features, suggesting an alternative mechanism.

The temporal source of the minimum in the HHG spectrum can be identified through the use of a time-frequency analysis (TFA). Through this analysis, windowed regions of the temporal domain of a signal are independently transformed to resolve the emergence of different frequencies in the signal. In the case shown in Fig. 10, a continuous wavelet analysis is used to transform a single recombination event occurring at the peak of the electric field, taking the form

$$C(t_0, \omega) = \frac{1}{\sqrt{2\pi}} \int_0^T d_{a_z}(t) W\left(\frac{\omega(t-t_0)}{2\pi}\right) dt, \quad (5)$$

where $W(x) = \frac{1}{\sqrt{\pi}} \exp(2\pi i x) \exp(-x^2)$ is the complex Morlet wavelet and $d_{a_z}(t)$ is the time-dependent dipole acceleration of the electron. The energy of the HHG minimum is noted by a horizontal black dashed line, and coincides with a time interval of suppressed emission in the TFA. Comparison of this emission feature with electron dynamics at the time of recombination is a straightforward procedure of analyzing computed observables on the same time interval as the TFA; however, a causative effect is not found. Instead, it is productive to consider electron behavior throughout ionization. This behavior can be constructed by conducting the classical association depicted in Fig. 10(c), assuming that the electron propagates as a point charge in the presence of an oscillatory electric field. In Fig. 10(d), the electron density at the time of ionization is reconstructed, and we observe that the electron is localized in the downhill (nonionizing) well at times corresponding to a reduction in the HHG signal. This interval of decreased ionization suppresses certain classical trajectories, which are then absent during recombination; the total HHG signal reflects this suppression through a modulation of the high-energy plateau. The fingerprint of transiently suppressed ionization in the HHG spectrum additionally represents a direct measurement of electron dynamics on an attosecond time scale.

It has been further shown [71] that changes in the nonadiabatic electron dynamics from cycle to cycle during the laser pulse may be traced using the emitted high harmonic signal by mimicking the experimental application of the attosecond light house technique [72,73] via the performance of windowed Fourier transforms. The spectral signals of individual recombination events show an increasing number of minima at different spectral locations, indicating a transition from adiabatic to nonadiabatic electron dynamics.

5. SUMMARY

In this review, we have presented a history of observations of nonadiabatic electron dynamics emerging from molecular systems driven by intense femtosecond laser fields. These nonadiabatic physics have been seen to modify ionization and fragmentation behavior in large molecular systems driven by mid-IR laser fields. Theoretical descriptions of multi-electron nonadiabatic effects have focused upon orbital coupling and modifications of the charge distribution as a primary characteristic of the response,

and have predicted the emergence of novel spectral features in ATI and HHG spectra.

In addition to these multi-electron studies, H_2^+ has proven an exceptional model system for simulating the nonadiabatic features found in larger molecules. When dissociating, H_2^+ passes through a regime of internuclear distances that are accompanied by near degeneracy of the ground and first excited state. The strong coupling of these states to the driving laser field enhances ionization rates and induces transient localization of the electron wavepacket, mimicking the charge density modulation theoretically observed in larger molecules and the increased ionization experimentally reported.

The capacity for H_2^+ to reproduce nonadiabatic dynamics was further explored as a means of testing the influence of nonadiabatic electron dynamics upon common signatures of strong-field physics. In particular, transient electron localization was shown to strongly alter fragmentation behavior upon molecular dissociation, to modify photoelectron distributions after laser-induced ionization, and to modulate the high-energy plateau of HHG, introducing spectral minima reflective of transiently suppressed ionization.

The findings reported throughout this review illustrate the importance of characterizing nonadiabatic electron behavior toward future efforts to control and image electrons in molecular systems. On the other hand, they also suggest an opportunity to more easily resolve dynamics on an attosecond time scale and manipulate electron distributions *in situ*. As advances in laser technologies introduce the capacity to promote nonadiabatic behaviors by driving systems with mid-IR wavelengths, these features offer an avenue to investigate and explore a rich array of physical effects.

Funding. National Science Foundation (NSF) (CNS-0821794, DGE 1144083, PHY 1068706, PHY 1125844); U.S. Department of Energy (DOE) (DE-FG02-09ER16103).

Acknowledgment. We appreciate collaborations and discussions with many colleagues on the topics presented in this review, including A. D. Bandrauk, S. L. Chin, R. Dörner, F. He, H. Kono, N. Takemoto, and U. Thumm.

REFERENCES

1. F. H. M. Faisal, *Theory of Multiphoton Process* (Plenum, 1987).
2. P. Agostini, F. Fabre, G. Mainfray, G. Petite, and N. K. Rahman, "Free-free transitions following six-photon ionization of xenon atoms," *Phys. Rev. Lett.* **42**, 1127–1130 (1979).
3. A. McPherson, G. Gibson, H. Jara, U. Johann, T. S. Luk, I. A. McIntyre, K. Boyer, and C. K. Rhodes, "Studies of multiphoton production of vacuum-ultraviolet radiation in the rare gases," *J. Opt. Soc. Am. B* **4**, 595–601 (1987).
4. X. F. Li, A. L'Huillier, M. Ferray, L. A. Lompre, and G. Mainfray, "Multiple-harmonic generation in rare gases at high laser intensity," *Phys. Rev. A* **39**, 5751–5754 (1989).
5. B. Walker, B. Sheehy, L. F. Di Mauro, P. Agostini, K. J. Schafer, and K. C. Kulander, "Precision measurement of strong field double ionization of helium," *Phys. Rev. Lett.* **73**, 1227–1230 (1994).
6. A. Talebpour, C.-Y. Chien, Y. Liang, S. Larochelle, and S. L. Chin, "Non-sequential ionization of Xe and Kr in an intense femtosecond Ti:sapphire laser pulse," *J. Phys. B* **30**, 1721–1730 (1997).
7. L. V. Keldysh, "Ionization in the field of a strong electromagnetic wave," *Sov. Phys. JETP* **20**, 1307–1314 (1965).
8. F. H. M. Faisal, "Multiple absorption of laser photons by atoms," *J. Phys. B* **6**, L89–L92 (1973).
9. H. R. Reiss, "Effect of an intense electromagnetic field on a weakly bound system," *Phys. Rev. A* **22**, 1786–1813 (1980).

10. A. M. Perelomov, S. V. Popov, and M. V. Terent'ev, "Ionization of atoms in an alternating electric field," *Sov. Phys. JETP* **23**, 924–934 (1966).
11. M. V. Ammosov, N. B. Delone, and V. P. Krainov, "Tunnel ionization of complex atoms and of atomic ions in an alternating electromagnetic field," *Sov. Phys. JETP* **64**, 1191–1194 (1986).
12. J. Muth-Böhm, A. Becker, and F. H. M. Faisal, "Suppressed molecular ionization for a class of diatomics in intense femtosecond laser fields," *Phys. Rev. Lett.* **85**, 2280–2283 (2000).
13. A. Jaroń-Becker, A. Becker, and F. H. M. Faisal, "Saturated ionization of fullerenes in intense laser fields," *Phys. Rev. Lett.* **96**, 143006 (2006).
14. T. Zuo and A. D. Bandrauk, "Charge-resonance-enhanced ionization of diatomic molecular ion by intense laser fields," *Phys. Rev. A* **52**, R2511–R2514 (1995).
15. T. Seideman, M. Y. Ivanov, and P. B. Corkum, "Role of electron localization in intense-field molecular ionization," *Phys. Rev. Lett.* **75**, 2819–2822 (1995).
16. M. Lezius, V. Blanchet, D. M. Rayner, D. M. Villeneuve, A. Stolow, and M. Y. Ivanov, "Nonadiabatic multielectron dynamics in strong field molecular ionization," *Phys. Rev. Lett.* **86**, 51–54 (2001).
17. M. Lezius, V. Blanchet, M. Y. Ivanov, and A. Stolow, "Polyatomic molecules in strong laser fields: nonadiabatic multielectron dynamics," *J. Chem. Phys.* **117**, 1575–1588 (2002).
18. A. Stolow, "The three pillars of photo-initiated quantum molecular dynamics," *Faraday Discuss.* **163**, 9–32 (2013).
19. A. N. Markevitch, S. M. Smith, D. A. Romanov, H. B. Schlegel, M. Y. Ivanov, and R. J. Levis, "Nonadiabatic dynamics of polyatomic molecules and ions in strong laser fields," *Phys. Rev. A* **68**, 011402 (R) (2003).
20. A. N. Markevitch, D. A. Romanov, S. M. Smith, H. B. Schlegel, M. Y. Ivanov, and R. J. Levis, "Sequential nonadiabatic excitation of large molecules and ions driven by strong laser fields," *Phys. Rev. A* **69**, 013401 (2004).
21. X. Li, S. M. Smith, A. N. Markevitch, D. A. Romanov, R. J. Levis, and H. B. Schlegel, "A time-dependent Hartree-Fock approach for studying the electronic optical response of molecules in intense fields," *Phys. Chem. Chem. Phys.* **7**, 233–239 (2005).
22. S. M. Smith, X. Li, A. N. Markevitch, D. A. Romanov, R. J. Levis, and H. B. Schlegel, "A numerical simulation of nonadiabatic electron excitation in the strong field regime: linear polyenes," *J. Phys. Chem. A* **109**, 5176–5185 (2005).
23. S. M. Smith, X. Li, A. N. Markevitch, D. A. Romanov, R. J. Levis, and H. B. Schlegel, "Numerical simulation of nonadiabatic electron excitation in the strong field regime. 2. Linear polyene cations," *J. Phys. Chem. A* **109**, 10527–10534 (2005).
24. S. M. Smith, X. Li, A. N. Markevitch, D. Romanov, R. J. Levis, and H. B. Schlegel, "Numerical simulation of nonadiabatic electron excitation in the strong field regime. 3. Polyacene neutrals and cations," *J. Phys. Chem. A* **111**, 6920–6932 (2007).
25. H. B. Schlegel, S. M. Smith, and X. Li, "Electronic optical response of molecules in intense fields: comparison of TD-HF, TD-CIS, and TD-CIS(D) approaches," *J. Chem. Phys.* **126**, 244110 (2007).
26. S. M. Smith, D. A. Romanov, X. Li, J. A. Sonk, H. B. Schlegel, and R. J. Levis, "Numerical bound state electron dynamics of carbon dioxide in the strong-field regime," *J. Phys. Chem. A* **114**, 2576–2587 (2010).
27. M. Spanner, J. Mikosch, A. Gijsberten, A. E. Boguslavskiy, and A. Stolow, "Multielectron effects and nonadiabatic electronic dynamics in above threshold ionization and high-harmonic generation," *New J. Phys.* **13**, 093010 (2011).
28. Y. Xia and A. Jaroń-Becker, "Fractional harmonics due to Mollow sidebands in high-order harmonic spectra of open-shell molecules at equilibrium geometries," (submitted).
29. B. R. Mollow, "Power spectrum of light scattered by two-level systems," *Phys. Rev.* **188**, 1969–1975 (1969).
30. T. Zuo, S. Chelkowski, and A. D. Bandrauk, "Harmonic generation by the H_2^+ molecular ion in intense laser fields," *Phys. Rev. A* **48**, 3837–3844 (1993).
31. T. Zuo, S. Chelkowski, and A. D. Bandrauk, "Photon-emission spectra of the H_2^+ molecular ion in an intense laser field," *Phys. Rev. A* **49**, 3943–3953 (1994).
32. R. S. Mulliken, "Intensities of electronic transitions in molecular spectra II. Charge-transfer spectra," *J. Chem. Phys.* **7**, 20–34 (1939).
33. I. Bocharova, R. Karimi, E. F. Penka, J.-P. Brichta, P. Lassonde, X. Fu, J.-C. Kieffer, A. D. Bandrauk, I. Litvinyuk, J. Sanderson, and F. Legare, "Charge resonance enhanced ionization of CO_2 probed by laser Coulomb explosion imaging," *Phys. Rev. Lett.* **107**, 063201 (2011).
34. S. Chelkowski, A. Conjusteau, T. Zuo, and A. Bandrauk, "Dissociative ionization of H_2^+ in an intense laser field: charge-resonance-enhanced ionization, Coulomb explosion, and harmonic generation at 600 nm," *Phys. Rev. A* **54**, 3235–3244 (1996).
35. H. Xu, F. He, D. Kielbinski, R. T. Sang, and I. V. Litvinyuk, "Experimental observation of the elusive double-peak structure in R-dependent strong-field ionization rate of H_2^+ ," *Sci. Rep.* **5**, 13527 (2015).
36. X.-B. Bian and A. D. Bandrauk, "Probing nuclear motion by frequency modulation of molecular high-order harmonic generation," *Phys. Rev. Lett.* **113**, 193901 (2014).
37. C. Huang, P. Lan, Y. Zhou, Q. Zhang, K. Liu, and P. Lu, "Tunneling site of electrons in strong-field-enhanced ionization of molecules," *Phys. Rev. A* **90**, 043420 (2014).
38. I. Kawata, H. Kono, and Y. Fujimura, "Adiabatic and diabatic responses of H_2^+ to an intense femtosecond laser pulse: dynamics of the electronic and nuclear wave packet," *J. Chem. Phys.* **110**, 11152–11165 (1999).
39. N. Takemoto and A. Becker, "Multiple ionization bursts in laser-driven hydrogen molecular ion," *Phys. Rev. Lett.* **105**, 203004 (2010).
40. N. Takemoto and A. Becker, "Time-resolved view on charge-resonance-enhanced ionization," *Phys. Rev. A* **84**, 023401 (2011).
41. N. Takemoto and A. Becker, "Visualization and interpretation of attosecond electron dynamics in laser-driven hydrogen molecular ion using Bohmian trajectories," *J. Chem. Phys.* **134**, 074309 (2011).
42. F. He, A. Becker, and U. Thumm, "Strong-field modulated diffraction effects in the correlated electron-nuclear motion in dissociating H_2^+ ," *Phys. Rev. Lett.* **101**, 213002 (2008).
43. A. Santana, J. M. Gomez Llorente, and V. Delgado, "Semiclassical dressed states of two-level quantum systems driven by non-resonant and/or strong laser fields," *J. Phys. B* **34**, 2371–2382 (2001).
44. G. L. Yudin, S. Chelkowski, J. Itatani, A. D. Bandrauk, and P. B. Corkum, "Attosecond photoionization of coherently coupled electronic states," *Phys. Rev. A* **72**, 051401(R) (2005).
45. S. Gräfe, V. Engel, and M. Y. Ivanov, "Attosecond photoelectron spectroscopy of electron tunneling in a dissociating hydrogen molecular ion," *Phys. Rev. Lett.* **101**, 103001 (2008).
46. H. D. Cohen and U. Fano, "Interference in the photo-ionization of molecules," *Phys. Rev.* **150**, 30–33 (1966).
47. T. Young, "The Bakerian lecture: on the theory of light and colours," *Philos. Trans. R. Soc.* **92**, 12–48 (1802).
48. P. Eckle, M. Smolarski, P. Schlup, J. Biegert, A. Staudte, M. Schöffler, J. G. Müller, R. Dörner, and U. Keller, "Attosecond angular streaking," *Nat. Phys.* **4**, 565–570 (2008).
49. M. Odenweller, N. Takemoto, A. Vredenburg, K. Cole, K. Pahl, J. Titze, L. P. Schmidt, T. Jahnke, R. Dörner, and A. Becker, "Strong field emission from fixed in space H_2^+ ," *Phys. Rev. Lett.* **107**, 143004 (2011).
50. P.-L. He, N. Takemoto, and F. He, "Photoelectron momentum distributions of atomic and molecular systems in strong circularly or elliptically polarized laser fields," *Phys. Rev. A* **91**, 063413 (2015).
51. P. B. Corkum, "Plasma perspective on strong field multiphoton ionization," *Phys. Rev. Lett.* **71**, 1994–1997 (1993).
52. K. J. Schafer, B. Yang, L. F. DiMauro, and K. C. Kulander, "Above threshold ionization beyond the high harmonic cutoff," *Phys. Rev. Lett.* **70**, 1599–1602 (1993).
53. M. Lein, N. Hay, R. Velotta, J. P. Marangos, and P. L. Knight, "Interference effects in high-order harmonic generation with molecules," *Phys. Rev. A* **66**, 023805 (2002).
54. M. Lein, N. Hay, R. Velotta, J. P. Marangos, and P. L. Knight, "Role of the intramolecular phase in high-harmonic generation," *Phys. Rev. Lett.* **88**, 183903 (2002).
55. M. F. Ciappina, A. Becker, and A. Jaroń-Becker, "Multislit interference patterns in high-order harmonic generation in C_{60} ," *Phys. Rev. A* **76**, 063406 (2007).
56. J. Itatani, J. Levesque, D. Zeidler, H. Niikura, H. Pepin, J. C. Kieffer, P. B. Corkum, and D. M. Villeneuve, "Tomographic imaging of molecular orbitals," *Nature* **432**, 867–871 (2004).
57. T. Kanai, S. Minemoto, and H. Sakai, "Quantum interference during high-order harmonic generation from aligned molecules," *Nature* **435**, 470–474 (2005).
58. C. Vozzi, F. Calegari, E. Benedetti, J. P. Caumes, G. Sansone, S. Stagira, M. Nisoli, R. Torres, E. Heesel, N. Kajumba, J. P. Marangos,

- C. Altucci, and R. Velotta, "Controlling two-center interference in molecular high harmonic generation," *Phys. Rev. Lett.* **95**, 153902 (2005).
59. S. Baker, J. S. Robinson, C. A. Haworth, H. Teng, R. A. Smith, C. C. Chirila, M. Lein, J. W. G. Tisch, and J. P. Marangos, "Probing proton dynamics in molecules on an attosecond time scale," *Science* **312**, 424–427 (2006).
60. N. L. Wagner, A. Wüst, I. P. Christov, T. Popmintchev, X. Zhou, M. M. Murnane, and H. C. Kapteyn, "Monitoring molecular dynamics using coherent electrons from high harmonic generation," *Proc. Natl. Acad. Sci. U.S.A.* **103**, 13279–13285 (2006).
61. W. Boutu, S. Haessler, H. Merdij, P. Breger, G. Waters, M. Stankiewicz, L. J. Frasinski, R. Taieb, J. Caillat, A. Maquet, P. Manchicourt, B. Carre, and P. Salieres, "Coherent control of attosecond emission from aligned molecules," *Nat. Phys.* **4**, 545–549 (2008).
62. X. Zhou, R. Lock, W. Li, N. Wagner, M. M. Murnane, and H. C. Kapteyn, "Molecular recollision interferometry in high harmonic generation," *Phys. Rev. Lett.* **100**, 073902 (2008).
63. W. Li, X. Zhou, R. Lock, S. Patchkovskii, A. Stolow, H. C. Kapteyn, and M. M. Murnane, "Time-resolved dynamics in N_2O_2 probed using high harmonic generation," *Science* **322**, 1207–1211 (2008).
64. S. Baker, J. S. Robinson, M. Lein, C. C. Chirila, R. Torres, H. C. Bandulet, D. Comtois, J. C. Kieffer, D. M. Villeneuve, J. W. G. Tisch, and J. P. Marangos, "Dynamic two-center interference in high-order harmonic generation from molecules with attosecond nuclear motion," *Phys. Rev. Lett.* **101**, 053901 (2008).
65. C. Vozzi, M. Negro, F. Calegari, G. Sansone, M. Nisoli, S. De Silvestri, and S. Stagira, "Generalized molecular orbital tomography," *Nat. Phys.* **7**, 822–826 (2011).
66. O. Smirnova, Y. Mairesse, S. Patchkovskii, N. Dudovich, D. Villeneuve, P. Corkum, and M. Y. Ivanov, "High harmonic interferometry of multi-electron dynamics in molecules," *Nature* **460**, 972–977 (2009).
67. H. J. Wörner, J. B. Bertrand, P. Hockett, P. B. Corkum, and D. M. Villeneuve, "Controlling the interference of multiple molecular orbitals in high-harmonic generation," *Phys. Rev. Lett.* **104**, 233904 (2010).
68. H. J. Wörner, J. P. Bertrand, D. V. Kartashov, P. B. Corkum, and D. M. Villeneuve, "Following a chemical reaction using high-harmonic interferometry," *Nature* **466**, 604–607 (2010).
69. H. J. Wörner, J. B. Bertrand, B. Fabre, J. Higuette, H. Ruf, A. Dubrouil, S. Patchkovskii, M. Spanner, Y. Mairesse, V. Blanchet, E. Mevel, E. Constant, P. B. Corkum, and D. M. Villeneuve, "Conical intersection dynamics in NO_2 probed by homodyne high-harmonic spectroscopy," *Science* **334**, 208–212 (2011).
70. Z. Diveki, A. Camper, S. Haessler, T. Auguste, T. Ruchon, B. Carre, P. Salieres, R. Guichard, J. Caillat, A. Maquet, and R. Taieb, "Spectrally resolved multi-channel contributions to the harmonic emission in N_2 ," *New J. Phys.* **14**, 023062 (2012).
71. M. R. Miller, A. Jaroń-Becker, and A. Becker, "High harmonic spectroscopy of laser-driven nonadiabatic electron dynamics in the hydrogen molecular ion," *Phys. Rev. A* **93**, 013406 (2016).
72. H. Vincenti and F. Quéré, "Attosecond lighthouses: how to use spatio-temporally coupled light fields to generate isolated attosecond pulses," *Phys. Rev. Lett.* **108**, 113904 (2012).
73. J. A. Wheeler, A. Borot, S. Monchocé, H. Vincenti, A. Ricci, A. Malvache, R. Lopez-Martens, and F. Quéré, "Attosecond lighthouses from plasma mirrors," *Nat. Photonics* **6**, 829–833 (2012).